Truncation thresholds: a pair of spike detection thresholds computed using truncated probability distributions

Murat OKATAN[1,*]**, Mehmet KOCATÜRK**[2]

[1]Department of Biomedical Engineering, Faculty of Technology, Cumhuriyet University, Sivas, Turkey

[2]Department of Biomedical Engineering, Faculty of Engineering and Natural Sciences, İstanbul Medipol University, İstanbul, Turkey

Abstract: We describe a method for computing a pair of spike detection thresholds, called 'truncation thresholds', using truncated probability distributions, for extracellular recordings. In existing methods the threshold is usually set to a multiple of an estimate of the standard deviation of the noise in the recording, with the multiplication factor being chosen between 3 and 5 according to the researcher's preferences. Our method has the following advantages over these methods. First, because the standard deviation is usually estimated from the entire recording, which includes the spikes, it increases with firing rate. By contrast, truncation thresholds decrease in absolute value with increasing firing rate, thereby capturing more of the signal. Second, the parameters of the selected noise distribution are estimated more accurately by maximum likelihood fitting of the truncated distribution to the data delimited by the truncation thresholds. Third, the computation of the truncation thresholds is completely data-driven. It does not involve a user-defined multiplication factor. Fourth, methods that use a threshold that is proportional to the estimated standard deviation of the noise assume that the noise distribution is symmetrical around the mean. By contrast, truncation thresholds are not linked to each other by an assumption of symmetry about some axis. Fifth, existing methods do not verify that subthreshold data obey a noise distribution. Truncation thresholds, however, are defined by the fact that the distribution of the data they delimit is statistically indistinguishable, according to the Kolmogorov–Smirnov test, from a selected distribution, truncated at those thresholds. Application of the method is illustrated using recordings from cortical area M1 in awake behaving rats, as well as in simulated recordings. Source code and executables of a software suite that computes the truncation thresholds are provided for the case when the noise distribution is modeled as truncated normal.

Key words: Biomedical signal processing, brain–machine interfaces, microelectrode recordings, computational neuroscience

1. Introduction

Extracellular recordings of neuronal activity provide information about the electrical activity of both individual and populations of neurons [1,2]. Extracellular recordings are widely used in behavioral neuroscience in exploring the information processing that takes place at the level of individual and populations of neurons [3]. In humans, such recordings are usually performed in the clinical setting, as in perioperative investigations in epilepsy [4] or in the use of brain–machine interfaces in patients with spinal cord injuries [5].

In most studies, the detection of action potentials, or spikes, constitutes one of the first steps in the use of

---

*Correspondence: muratokatan@cumhuriyet.edu.tr

extracellular neural recordings [6]. Because spikes stand out in these data as relatively large amplitude events, the easiest and most straightforward method for detecting them is amplitude thresholding. The threshold is usually set to $k \times \hat{\sigma}$, where $\hat{\sigma}$ is an estimate of the standard deviation of the noise in the recording and k is a multiplication factor that is usually chosen to be between 3 and 5 depending on the researcher's preferences [7–11]. However, this method of determining the threshold has some drawbacks. First, the use of such a multiplication factor (k) adds an element of subjectivity to spike detection. In addition, the standard deviation estimate ($\hat{\sigma}$) increases with the spiking frequency of the recorded neurons [7]. This is undesired since an increase in spiking frequency, or firing rate, does not necessarily imply an increase in the standard deviation of the noise that is present in the recording. As a consequence of the firing rate-dependent increase in both $\hat{\sigma}$ and the threshold that is proportional to $\hat{\sigma}$, more action potentials may be missed at high firing rates. Apart from the dependence on firing rate, choosing k high is likely to result in some action potentials being classified as noise, whereas choosing it low is likely to result in some noise events being classified as spike candidates. Evidence suggests that suprathreshold events carry information regardless of whether they can be identified as individual spikes [11]. These findings and observations underline the importance of using an objective and accurate method for computing spike detection thresholds that can efficiently separate signal and noise. Accordingly, this study addresses the question of whether spikes in extracellular recordings can be detected through thresholding in a principled way that is completely independent of the researcher. To address this issue, a method of computing a pair of spike detection thresholds, called 'truncation thresholds', is developed, and its application is illustrated in extracellular recordings obtained from cortical area M1 in awake behaving rats, as well as in simulated spike trains. The method has general applicability to problems where a continuous-valued data set needs to be segmented into two nonoverlapping parts such that one part obeys a desired continuous-valued truncated distribution while the other does not. Preliminary results of this study have been published in [12,13].

2. Materials and methods

This section explains the computation of the truncation thresholds along with the real and simulated neural data that are used for illustrating their application. All computations were performed in MATLAB (R2015a, MathWorks, Inc., USA) under a 64 bit Windows 8.1 Single Language (2013) operating system on a laptop computer with 6 GB RAM and 2.60 GHz Intel®Core™i5-3230M CPU.

2.1. Mathematical representation of the recordings

Because extracellular neural recordings are typically acquired using analog to digital conversion systems, their initial representation in digital form is a discrete-time discrete-valued time series. Let $d[n]$, $0 \leq n \leq N - 1$, denote such a recording, with N representing the total number of samples in the recording. The method presented here computes the spike detection thresholds by verifying that the samples that lie between the thresholds obey a truncated continuous-valued probability distribution function. This verification is performed using the Kolmogorov–Smirnov (KS) test. Because $d[n]$ is discrete-valued, the distribution of its samples will likely deviate significantly from a continuous distribution for any reasonable choice of thresholds, which implies that the method proposed here may not be applied directly on $d[n]$. Fortunately, spike detection is usually not performed directly on $d[n]$, but rather on a band-pass filtered version of it, in which frequencies below a few hundred Hz and above a few kHz are attenuated. This filtering is expected to convert $d[n]$ into a time series that can be considered continuous-valued for the purposes of the present method. Let $x[n]$ denote this filtered recording. The following analysis assumes that the spikes will be detected in $x[n]$ and that $x[n]$ is a continuous-valued discrete-time signal.

2.2. Basic premises of truncation thresholds

Extracellular recordings are often assumed to consist of background activity and action potentials, or spikes. The background activity is assumed to arise from the superimposed electrical activities of large numbers of neurons that are located at various distances relative to the recording electrode and that are usually asynchronous. Therefore, background activity is usually considered noise [7,14,15]. Consistent with this characterization, the present analysis assumes that there exist threshold pairs $\Theta = [\theta_l, \theta_h]$, $min(x) \leq \theta_l < \theta_h \leq max(x)$, such that the samples that are between these thresholds, $z_\Theta \in \{x[n] \mid \theta_l \leq x[n] \leq \theta_h\}$, obey a parametric continuous-valued noise distribution $F\left(z \mid \hat{\zeta}_\Theta\right)$ that is truncated at θ_l and θ_h, where $\hat{\zeta}_\Theta$ is the parameter vector that is estimated from z_Θ by maximum likelihood. Note that each selection of Θ defines a z_Θ and a $\hat{\zeta}_\Theta$. It is accepted that the truncated distribution $F\left(z \mid \hat{\zeta}_\Theta\right)$ fits the truncated data if the KS test yields a P-value that is at least α. Clearly, for any choice of Θ, a KS P-value is obtained. Let $P_{KS}(\Theta)$ denote this value. The largest amount of noise, under $F\left(z \mid \hat{\zeta}_\Theta\right)$, is segmented out of x, by the value of Θ that maximizes $\Delta(\Theta) \triangleq \theta_h - \theta_l$ and for which $P_{KS}(\Theta) \geq \alpha$. Let this optimal solution be denoted by $\hat{\Theta}_o$. Since x is assumed to be continuous-valued, it may contain about N distinct values, each of which is a candidate for θ_l or θ_h. Thus, it may be presumed that there are about $N(N-1)/2$ different choices of Θ that need to be evaluated in order to find $\hat{\Theta}_o$. For any recording of practical use, this number is prohibitively large. Therefore, rather than aiming at the optimal solution by evaluating all possible values of Θ, a method needs to be adopted that yields a solution with large $\Delta(\Theta)$ and that can be computed relatively faster. The method presented here computes such a solution, and the resulting thresholds, denoted by $\hat{\Theta}_t$, are called 'truncation thresholds'.

The computation of $\hat{\Theta}_t$ involves two steps. In the first step, initial values for the lower and upper thresholds are computed using the bisection method [16] under the constraint that the other threshold is fixed at the median of x. That is, $\hat{\Theta}_{l|m} \triangleq \left[\hat{\theta}_{l|m}, median(x)\right]$ and $\hat{\Theta}_{h|m} \triangleq \left[median(x), \hat{\theta}_{h|m}\right]$ values are computed as explained in Section 2.3. In the second step the interval $\left[\hat{\theta}_{l|m}, \hat{\theta}_{h|m}\right]$ is stretched or compressed, anchored at the median, using the bisection method, to yield $\hat{\Theta}_t$, as explained in Section 2.4. The median is used as an anchor because it is expected to be located near the middle of the background activity given that the greater part of x is due to the background activity. Because an ordered threshold pair can also be viewed as an interval, it will be referred to as one when appropriate.

2.3. Computing initial values for the lower and upper thresholds

The lower threshold in $\hat{\Theta}_{l|m}$, $\hat{\theta}_{l|m}$, is searched using the bisection method in a set of candidate solutions that is reduced down to half of its size after each bisection. The initial value of this set is defined as $SCS_{l|m}[1] = \{x[n] \mid x[n] < median(x)\}$. The solution is obtained after at most I iterations, where I is the smallest integer that is greater than or equal to $log_2(K)$ and K is the cardinality of $SCS_{l|m}[1]$.

The solution candidate at iteration i is defined as $\theta_{l|m}[i]$, which is the sample that is closest to $median\left(SCS_{l|m}[i]\right)$. This yields the threshold pair $\Theta_{l|m}[i] = \left[\theta_{l|m}[i], median(x)\right]$. If $P_{KS}\left(\Theta_{l|m}[i]\right) \geq \alpha$, then the data that lie in the interval $\Theta_{l|m}[i]$ are accepted to obey the truncated noise distribution $F\left(z \mid \hat{\zeta}_{A[i]}\right)$, where $A[i] = \Theta_{l|m}[i]$. This implies that the search for the solution can continue in the set $SCS_{l|m}[i+1] =$

$\{x\,[n] \in SCS_{l|m}\,[i]\,|\,x\,[n] < \theta_{l|m}\,[i]\}$. If, however, $P_{KS}\left(\Theta_{l|m}\,[i]\right) < \alpha$, then the data that lie in the interval $\Theta_{l|m}\,[i]$ are not accepted to obey $F\left(z\,|\,\hat{\zeta}_{A[i]}\right)$. This implies that the search for the solution can continue in the set $SCS_{l|m}\,[i+1] = \left\{x\,[n] \in SCS_{l|m}\,[i]\,|\,x\,[n] > \theta_{l|m}\,[i]\right\}$. This iterative search continues until the cardinality of the set of candidate solutions becomes zero. After the iteration terminates, a search is conducted over all solution candidates $\Theta_{l|m}\,[i]$, $1 \leq i \leq I$, to find the one that maximizes $\Delta\left(\Theta_{l|m}\,[i]\right)$ and for which $P_{KS}\left(\Theta_{l|m}\,[i]\right) \geq \alpha$. Let $\hat{\Theta}_{l|m}$ denote this solution.

The upper threshold in $\hat{\Theta}_{h|m}$, $\hat{\theta}_{h|m}$, is searched in a similar manner. This time the initial value of the set of candidate solutions is defined as $SCS_{h|m}\,[1] = \{x\,[n]\,|\,x\,[n] > median\,(x)\}$. The solution is obtained after at most J iterations, where J is the smallest integer that is greater than or equal to $log_2\,(L)$ and L is the cardinality of $SCS_{h|m}\,[1]$. The solution candidate at iteration i is defined as $\theta_{h|m}\,[i]$, which is the sample that is closest to $median\left(SCS_{h|m}\,[i]\right)$. This yields the threshold pair $\Theta_{h|m}\,[i] = \left[median\,(x),\,\theta_{h|m}\,[i]\right]$. If $P_{KS}\left(\Theta_{h|m}\,[i]\right) \geq \alpha$, then the data that lie in the interval $\Theta_{h|m}\,[i]$ are accepted to obey the truncated noise distribution $F\left(z\,|\,\hat{\zeta}_{B[i]}\right)$, where $B[i] = \Theta_{h|m}\,[i]$. This implies that the search for the solution can continue in the set $SCS_{h|m}\,[i+1] = \left\{x\,[n] \in SCS_{h|m}\,[i]\,|\,x\,[n] > \theta_{h|m}\,[i]\right\}$. If, however, $P_{KS}\left(\Theta_{h|m}\,[i]\right) < \alpha$, then the data that lie in the interval $\Theta_{h|m}\,[i]$ are not accepted to obey $F\left(z\,|\,\hat{\zeta}_{B[i]}\right)$. This implies that the search for the solution can continue in the set $SCS_{h|m}\,[i+1] = \left\{x\,[n] \in SCS_{h|m}\,[i]\,|\,x\,[n] < \theta_{h|m}\,[i]\right\}$. This iterative search continues until the cardinality of the set of candidate solutions becomes zero. After the iteration terminates, a search is conducted over all solution candidates $\Theta_{h|m}\,[i]$, $1 \leq i \leq J$, to find the one that maximizes $\Delta\left(\Theta_{h|m}\,[i]\right)$ and for which $P_{KS}\left(\Theta_{h|m}\,[i]\right) \geq \alpha$. Let $\hat{\Theta}_{h|m}$ denote this solution.

If both $P_{KS}\left(\Theta_{l|m}\,[i]\right) < \alpha$ for $1 \leq i \leq I$ and $P_{KS}\left(\Theta_{h|m}\,[i]\right) < \alpha$ for $1 \leq i \leq J$, then neither $\hat{\Theta}_{l|m}$ nor $\hat{\Theta}_{h|m}$ could be found, which implies that $\hat{\Theta}_t$ could not be found either. If only $\hat{\Theta}_{l|m}$ or $\hat{\Theta}_{h|m}$ is found, then the one that is found equals $\hat{\Theta}_t$. If both $\hat{\Theta}_{l|m}$ and $\hat{\Theta}_{h|m}$ are found, then $\hat{\Theta}_t$ is computed as explained next.

2.4. Computing the truncation thresholds from the initial values

The threshold pairs $\hat{\Theta}_{l|m}$ and $\hat{\Theta}_{h|m}$ represent two intervals, below and above $median\,(x)$ respectively, in which the data obey the respective truncated distributions with $P_{KS}\left(\hat{\Theta}_{l|m}\right) \geq \alpha$ and $P_{KS}\left(\hat{\Theta}_{h|m}\right) \geq \alpha$. The goal of the present analysis is to find a single pair of thresholds $\hat{\Theta}_t \triangleq \left[\hat{\theta}_{t1},\,\hat{\theta}_{t2}\right]$, that will be a wide interval in which the data obey the respective truncated distribution with $P_{KS}\left(\hat{\Theta}_t\right) \geq \alpha$. This interval is constructed by merging the intervals $\hat{\Theta}_{l|m}$ and $\hat{\Theta}_{h|m}$ and then scaling the resulting interval, anchored at the median, by the bisection method, as explained next.

First, the threshold pair $\hat{\Theta}_w \triangleq \left[\hat{\theta}_{l|m},\hat{\theta}_{h|m}\right]$ is obtained by using the lower and upper thresholds in $\hat{\Theta}_{l|m}$ and $\hat{\Theta}_{h|m}$ respectively, and its adequacy is assessed. The search for the truncation thresholds proceeds differently depending on whether $P_{KS}\left(\hat{\Theta}_w\right) \geq \alpha$.

2.4.1. Computation of the truncation thresholds when $P_{KS}\left(\hat{\Theta}_{w}\right) \geq \alpha$

If $P_{KS}\left(\hat{\Theta}_{w}\right) \geq \alpha$, then it is inferred that the interval $\hat{\Theta}_{w}$ can be widened, unless it already is the widest possible interval. $\hat{\Theta}_{w}$ is the widest possible interval if $\hat{\Theta}_{w} = [min(x), max(x)]$. In that case the truncation thresholds are found as $\hat{\Theta}_{t} = \hat{\Theta}_{w} = \hat{\Theta}_{o}$. If $\hat{\Theta}_{w}$ is not the widest possible interval, however, then it is inferred that the truncation thresholds may correspond to an interval that is wider than $\hat{\Theta}_{w}$. In that case $\hat{\Theta}_{t}$ is computed as $\Theta_{t}\left(\hat{\phi}\right)$ using Eq. (1), where $\hat{\phi}$ is a factor that is determined from the data by the bisection method, as explained next.

$$\Theta_{t}(\phi) = (1 - \phi) \times median(x) + \phi \times \hat{\Theta}_{w} \tag{1}$$

Since the role of $\Theta_{t}(\phi)$ is to partition the samples in x into two classes, one noise and the other nonnoise, it suffices if the upper or the lower threshold in $\Theta_{t}(\phi)$, or both, are in $\{x[n] \mid x[n] \neq median(x)\}$. Let S_{l+}, defined in Eq. (2), denote the set of factors that adjust the lower threshold to any of the samples in x that are smaller than $\hat{\theta}_{l|m}$:

$$S_{l+} = \left\{ \frac{median(x) - x[n]}{median(x) - \hat{\theta}_{l|m}} \mid x[n] < \hat{\theta}_{l|m} \right\} \tag{2}$$

Let S_{h+}, defined in Eq. (3), denote the set of factors that adjust the upper threshold to any of the samples in x that are greater than $\hat{\theta}_{h|m}$:

$$S_{h+} = \left\{ \frac{x[n] - median(x)}{\hat{\theta}_{h|m} - median(x)} \mid x[n] > \hat{\theta}_{h|m} \right\} \tag{3}$$

Then the set of candidate solutions for ϕ is defined in Eq. (4) at the first iteration of the bisection method:

$$SCS_{m+}[1] = S_{l+} \cup S_{h+} \tag{4}$$

The solution for ϕ is obtained after at most M iterations, where M is the smallest integer that is greater than or equal to $log_{2}(Q)$ and Q is the cardinality of $SCS_{m+}[1]$.

The solution candidate at iteration i is defined as $\phi[i]$, which is the element of $SCS_{m+}[i]$ that is closest to $median(SCS_{m+}[i])$. This yields the threshold pair $\Theta_{t}(\phi[i])$. If $P_{KS}(\Theta_{t}(\phi[i])) \geq \alpha$, then the data that lie in the interval $\Theta_{t}(\phi[i])$ are accepted to obey the truncated noise distribution $F\left(z \mid \hat{\zeta}_{C[i]}\right)$, where $C[i] = \Theta_{t}(\phi[i])$. This implies that the search for the solution can continue in the set $SCS_{m+}[i+1] = \{\phi \in SCS_{m+}[i] \mid \phi > \phi[i]\}$. If, however, $P_{KS}(\Theta_{t}(\phi[i])) < \alpha$, then the data that lie in the interval $\Theta_{t}(\phi[i])$ are not accepted to obey $F\left(z \mid \hat{\zeta}_{C[i]}\right)$. This implies that the search for the solution can continue in the set $SCS_{m+}[i+1] = \{\phi \in SCS_{m+}[i] \mid \phi < \phi[i]\}$. This iterative search continues until the cardinality of the set of candidate solutions becomes zero. After the iteration terminates, a search is conducted over all solution candidates $\phi[i]$, $1 \leq i \leq M$, to find the one that maximizes $\Delta(\Theta_{t}(\phi[i]))$ and for which $P_{KS}(\Theta_{t}(\phi[i])) \geq \alpha$. Let $\hat{\phi}$ denote this solution. If $P_{KS}(\Theta_{t}(\phi[i])) < \alpha$ for $1 \leq i \leq M$, then it is inferred that $\hat{\phi} = 1$, since $P_{KS}\left(\hat{\Theta}_{w}\right) \geq \alpha$. Let $\hat{\Theta}_{t} = \Theta_{t}\left(\hat{\phi}\right)$ denote the associated threshold pair, which are called 'truncation thresholds'.

2.4.2. Computation of the truncation thresholds when $\mathbf{P_{KS}}\left(\hat{\Theta}_\mathbf{w}\right) < \alpha$

If $P_{KS}\left(\hat{\Theta}_w\right) < \alpha$, then it is inferred that the truncation thresholds may correspond to an interval that is narrower than $\hat{\Theta}_w$. In that case $\hat{\Theta}_t$ is computed as $\Theta_t\left(\hat{\phi}\right)$ using Eq. (1) with a set of candidate solutions that is constructed as follows. Let S_{l-}, defined in Eq. (5), denote the set of factors that adjust the lower threshold to any of the samples in x that are greater than $\hat{\theta}_{l|m}$ and smaller than the median:

$$S_{l-} = \left\{ \frac{median\,(x) - x\,[n]}{median\,(x) - \hat{\theta}_{l|m}} \,|\, \hat{\theta}_{l|m} < x\,[n] < median\,(x) \right\} \tag{5}$$

Let S_{h-}, defined in Eq. (6), denote the set of factors that adjust the upper threshold to any of the samples in x that are smaller than $\hat{\theta}_{h|m}$ and greater than the median:

$$S_{h-} = \left\{ \frac{x\,[n] - median\,(x)}{\hat{\theta}_{h|m} - median\,(x)} \,|\, median\,(x) < x\,[n] < \hat{\theta}_{h|m} \right\} \tag{6}$$

Then the set of candidate solutions for ϕ is defined in Eq. (7) at the first iteration of the bisection method:

$$SCS_{m-}\,[1] = S_{l-} \cup S_{h-} \tag{7}$$

The solution for ϕ is obtained after at most R iterations, where R is the smallest integer that is greater than or equal to $log_2\,(U)$ and U is the cardinality of $SCS_{m-}\,[1]$.

The solution candidate at iteration i is defined as $\phi\,[i]$, which is the element of $SCS_{m-}\,[i]$ that is closest to $median\,(SCS_{m-}\,[i])$. This yields the threshold pair $\Theta_t\,(\phi\,[i])$. If $P_{KS}\,(\Theta_t\,(\phi\,[i])) \geq \alpha$, then the search for the solution can continue in the set $SCS_{m-}\,[i+1] = \{\phi \in SCS_{m-}\,[i]\,|\,\phi > \phi\,[i]\}$. If, however, $P_{KS}\,(\Theta_t\,(\phi\,[i])) < \alpha$, then the search for the solution can continue in the set $SCS_{m-}\,[i+1] = \{\phi \in SCS_{m-}\,[i]\,|\,\phi < \phi\,[i]\}$. This iterative search continues until the cardinality of the set of candidate solutions becomes zero. After the iteration terminates, a search is conducted over all solution candidates $\phi\,[i]$, $1 \leq i \leq R$, to find the one that maximizes $\Delta\,(\Theta_t\,(\phi\,[i]))$ and for which $P_{KS}\,(\Theta_t\,(\phi\,[i])) \geq \alpha$. Let $\hat{\phi}$ denote this solution. Then the truncation thresholds are obtained again as $\hat{\Theta}_t = \Theta_t\left(\hat{\phi}\right)$. If $P_{KS}\,(\Theta_t\,(\phi\,[i])) < \alpha$ for $1 \leq i \leq R$, then it is inferred that truncation thresholds could not be found for x.

A software suite that computes the truncation thresholds by modeling the noise using the truncated normal distribution is available at scicrunch.org under RRID:SCR_014637

2.5. Application on real data

Computation of the truncation thresholds is illustrated using data that were recorded in a previous study. The recording was made using a neuroprosthesis design environment [17] from the primary motor cortex (area M1) of a rat during lever-pressing in response to visual stimuli. The data segment that is used here is about 12.6 s long and was recorded with a sampling rate of 40 kHz. It was then digitally band-pass filtered between 400 Hz and 8 kHz using a 4th order Butterworth filter.

A truncated normal probability distribution function (Eq. (8)) is used as the noise model $F\left(z \,|\, \hat{\zeta}_{\hat{\Theta}_t}\right)$, where $\hat{\zeta}_{\hat{\Theta}_t} = \left[\hat{\mu}_{\hat{\Theta}_t}, \hat{\sigma}_{\hat{\Theta}_t}\right]$ is the maximum likelihood estimate of the parameter vector consisting of the mean and the standard deviation. Here $\Phi\left(\cdot\right)$ is the cumulative standard normal distribution function.

$$F\left(z \,|\, \hat{\zeta}_{\hat{\Theta}_t}\right) = \left(\Phi\left(\frac{z - \hat{\mu}_{\hat{\Theta}_t}}{\hat{\sigma}_{\hat{\Theta}_t}}\right) - \Phi\left(\frac{\hat{\theta}_{t1} - \hat{\mu}_{\hat{\Theta}_t}}{\hat{\sigma}_{\hat{\Theta}_t}}\right)\right)\left(\Phi\left(\frac{\hat{\theta}_{t2} - \hat{\mu}_{\hat{\Theta}_t}}{\hat{\sigma}_{\hat{\Theta}_t}}\right) - \Phi\left(\frac{\hat{\theta}_{t1} - \hat{\mu}_{\hat{\Theta}_t}}{\hat{\sigma}_{\hat{\Theta}_t}}\right)\right)^{-1} \tag{8}$$

2.6. Application on simulated data

Simulated neural data were generated and analyzed to determine the dependence of truncation thresholds on firing rate. These analyses also revealed the accuracy with which $\hat{\sigma}_{\hat{\Theta}_t}$ estimates the noise standard deviation. Eq. (9) defines the simulated data, which were generated for firing rates f between 0 Hz and 50 Hz with steps of 5 Hz.

$$y_f\left[n\right] = g\left[n\right] + a_f\left[n\right] \tag{9}$$

Each y_f had a duration of 10 s and was sampled at 40 kHz. The noise was generated as the Gaussian process defined in Eq. (10)

$$g\left[n\right] \sim N\left(0, \sigma\right) \tag{10}$$

Here, $\sigma = \hat{\sigma}_{\hat{\Theta}_t}$ is the noise standard deviation estimated from the real data, as explained in Sections 2.2–2.5.

The spiking processes a_f were generated by repeating a single well-isolated spike, obtained from the real data, according to Poisson processes with specified frequencies. Truncation thresholds computed for y_f are denoted by $\hat{\Theta}_{t,f}$. These thresholds and thresholds proportional to estimated noise standard deviations are plotted as a function of f to illustrate their dependence on firing rate. A proportionality constant of $k = 4$ was used as a typical value (e.g., [7]). The two standard deviation estimators that are used in addition to $\hat{\sigma}_{\hat{\Theta}_{t,f}}$ are given in Eq. (11) [18] and Eq. (12), where $\hat{\mu}_f$ is the mean value of y_f.

$$\hat{\sigma}_{m,f} = median\left(|y_f|\right)\left(\Phi^{-1}\left(0.75\right)\right)^{-1} \tag{11}$$

$$\hat{\sigma}_f = \sqrt{\frac{1}{N}\sum_{n=0}^{N-1}\left(y_f\left[n\right] - \hat{\mu}_f\right)^2} \tag{12}$$

3. Results

Truncation thresholds are first computed for real extracellular neural activity data to show that they can be computed under the truncated normal distribution noise model. Next, the results on the firing rate dependence of truncation thresholds and alternative thresholds are illustrated using simulated data.

3.1. Truncation thresholds computed for real data

Figure 1 shows a portion of the real data that are used in this study. The duration of this interval is about 2 s and it is located near the middle of the whole recording. Spikes of various amplitudes are visible over a steady background activity. The two horizontal lines show the truncation thresholds that are computed for the whole

recording with $\alpha = 0.05$. The location of the truncation thresholds on the 1000 point normalized histogram of the data is also shown. Only the range between $\pm 100\,\mu V$ is shown for clarity. The number of samples in this recording was $N = 504,735$. Consequently, it took 18 iterations to compute each of $\hat{\theta}_{l|m}$ and $\hat{\theta}_{h|m}$, given that $log_2\left(N/2\right) = 17.9$. The values of $\theta_{l|m}\left[i\right]$ and $\theta_{h|m}\left[i\right]$ are shown in Figure 1 for $1 \le i \le 18$. $\hat{\theta}_{l|m}$ and $\hat{\theta}_{h|m}$ were found as $\theta_{l|m}\left[18\right] = -25.9\,\mu V$ and $\theta_{h|m}\left[16\right] = 23.2\,\mu V$, respectively. Upon evaluating $P_{KS}\left(\hat{\Theta}_w\right)$, it was found to be smaller than α, indicating that $\hat{\phi}$ needed to be searched in the set of candidate solutions defined in Eq. (7). The cardinality of this set was $U = 438,034$. Thus, it took 19 iterations to find $\hat{\phi}$, given that $log_2\left(U\right) = 18.7$. $\phi\left[i\right]$ and $\Theta_t\left[i\right]$ values are shown in Figure 1 for $1 \le i \le 19$. $\hat{\phi}$ was found as $\phi\left[18\right] = 0.90$. This resulted in $\hat{\Theta}_t = \left[-23.4,\ 20.9\right]\,\mu V$.
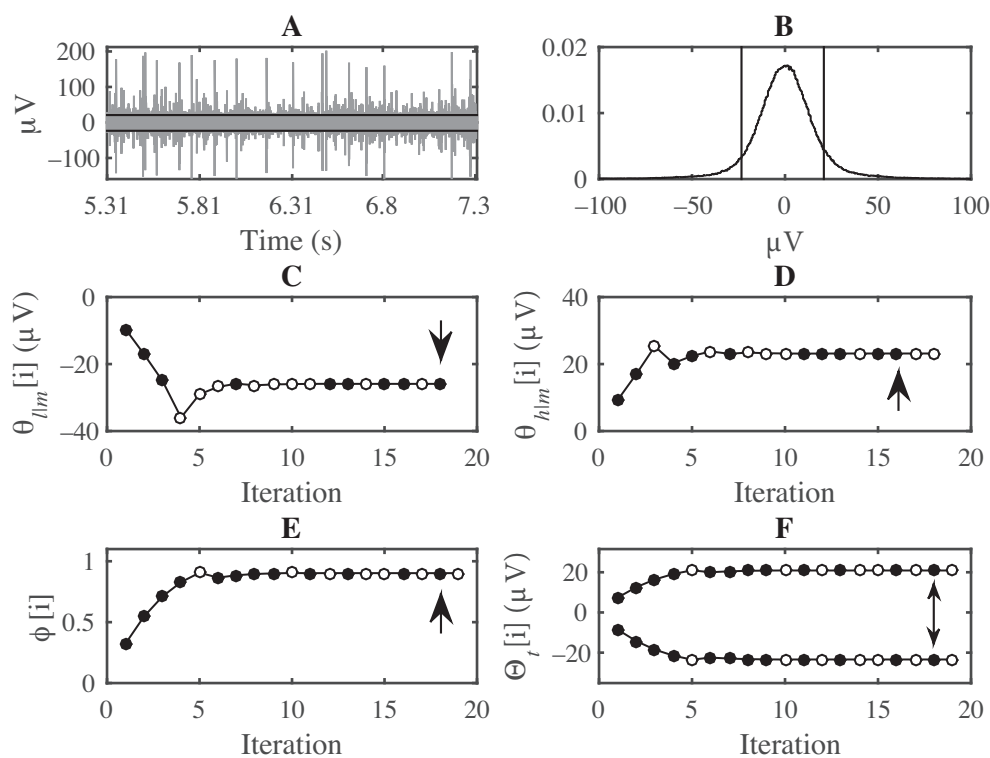

Figure 1. Computation of the truncation thresholds. (A) A segment of the real extracellular recording after filtering. Horizontal lines indicate the truncation thresholds. (B) Normalized 1000 point histogram of the samples that make up the filtered recording, shown in the interval $\pm 100\ \mu$V. Vertical lines indicate the truncation thresholds. (C–F) The values of $\theta_{l|m}\left[i\right]$, $\theta_{h|m}\left[i\right]$, $\phi\left[i\right]$, and $\Theta_t\left[i\right]$, respectively. Filled circles show solutions for which the KS test P-value is at least 0.05. Arrows indicate $\hat{\theta}_{l|m}$, $\hat{\theta}_{h|m}$, $\hat{\phi}$, and $\hat{\Theta}_t$.

3.2. Truncation thresholds computed for simulated data

Figure 2 shows the real action potential that was used in generating the simulated data. Segments of simulated data for firing rates of $f = 0$ Hz, 25 Hz, and 50 Hz are also shown in the figure along with the corresponding truncation thresholds superimposed on 1000 point normalized histograms. Truncation thresholds converged to the minimum and the maximum sample in the recording when $f = 0$ Hz.
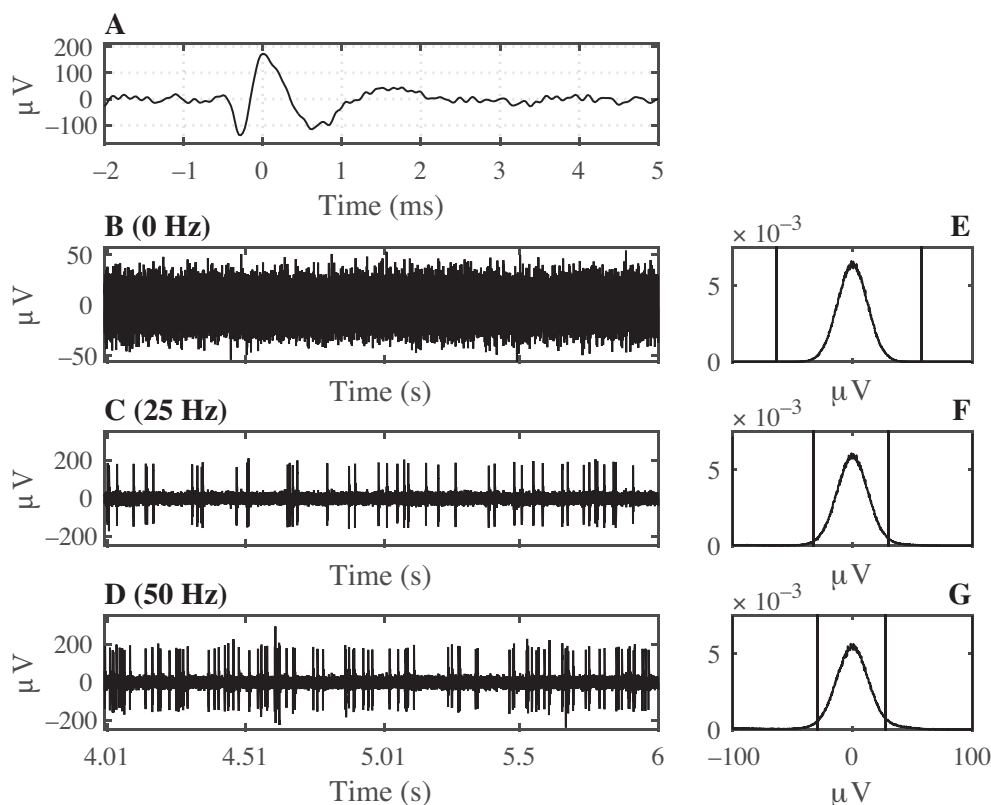
Figure 2. Generation and analysis of simulated data. (A) The well-isolated action potential that was used for generating the simulated spike trains. (B–D) The sum of simulated noise and spike trains at firing rates of 0 Hz, 25 Hz, and 50 Hz, respectively. Graphs show the central 2 s of 10 s long simulated data. (E–G) Normalized 1000 point histograms of the samples that make up the simulated data. Vertical lines indicate the truncation thresholds.

Figure 3 shows $\hat{\Theta}_{t,f}$, the truncation thresholds computed for the simulated data. For comparison $4 \times \hat{\sigma}_f$, $4 \times \hat{\sigma}_{m,f}$, $4 \times \hat{\sigma}_{\hat{\Theta}_{t,f}}$, and $4 \times \sigma$ curves are also plotted. It can be seen that $4 \times \hat{\sigma}_f$ and $4 \times \hat{\sigma}_{m,f}$ increase with increasing firing rate as expected [7]. Although $4 \times \hat{\sigma}_{\hat{\Theta}_{t,f}}$ also increases with firing rate, it increases slower than the latter two. All these thresholds start very close to $4 \times \sigma$ at $f = 0$ Hz. Unlike these thresholds, truncation thresholds exceed $\pm 4 \times \sigma$ at $f = 0$ Hz and decrease in absolute value with increasing firing rate.

4. Discussion

The most widely used method for computing spike detection thresholds is amplitude thresholding using thresholds that are proportional to estimated standard deviation of noise. Truncation thresholds overcome all of the known shortcomings of this method. The results show that truncation thresholds can be computed for real extracellular recordings by modeling the noise using the truncated normal probability distribution (Figure 1). The theory presented here allows computing these thresholds using other continuous-valued probability distributions as the noise model. Alternative models may be explored in future studies.

Analysis results of the simulated data (Figures 2 and 3) showed that the noise standard deviation estimator $\hat{\sigma}_{\hat{\Theta}_{t,f}}$, which is computed as a byproduct of the computation of the truncation thresholds, is more accurate than $\hat{\sigma}_f$ and $\hat{\sigma}_{m,f}$, which are estimators that are widely used in the literature. This implies that
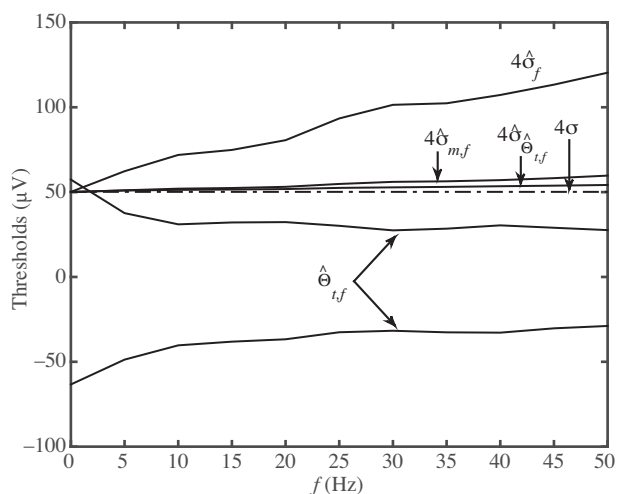
Figure 3. Firing rate dependence of truncation thresholds. Truncation thresholds ($\hat{\Theta}_{t,f}$) that are computed for the simulated recordings of varying firing rate (f) are observed to decrease in absolute value with increasing firing rate. By contrast, spike detection thresholds that are set to four times the estimated noise standard deviation increase with firing rate: $4 \times \hat{\sigma}_f$: from Eq. (12); $4 \times \hat{\sigma}_{m,f}$: from Eq. (11); $4 \times \hat{\sigma}_{\hat{\Theta}_{t,f}}$: from Eq. (8). Four times the actual value of the noise standard deviation is shown as a reference ($4 \times \sigma$, dashed horizontal line). $\hat{\sigma}_{\hat{\Theta}_{t,f}}$, which is estimated as part of the computation of the truncation thresholds, is observed to estimate σ more accurately than $\hat{\sigma}_f$ and $\hat{\sigma}_{m,f}$ at all firing rates.

the noise standard deviation in extracellular recordings can be estimated more accurately by using the method presented here.

Truncation thresholds accurately classified all samples in the simulated recording as noise when the simulated recording was indeed a pure noise process ($f = 0$ Hz in Figures 2 and 3). By contrast, the other thresholds misclassified some noise samples as signal, since the probability of crossing the threshold $4 \times \sigma$ is $1 - \Phi(4) \cong 3.2\,10^{-5}$. In view of the fact that the simulated recordings contained $N = 400,000$ samples, it is expected that about 13 samples will be above $4 \times \sigma$. Indeed, 18 samples were found to cross this threshold in the $f = 0$ Hz condition.

The decrease in the absolute value of the truncation thresholds with firing rate (Figures 2 and 3) shows that these thresholds allow more of the signal (action potential waveforms) to be classified as signal rather than noise as the firing rate increases. This is exactly what is needed by downstream applications that extract information from the suprathreshold data. In this regard, truncation thresholds have a clear advantage over the alternative thresholds considered here, because the latter increase with firing rate. Since truncation thresholds define the limits of the data that obey the truncated noise distribution, suprathreshold samples do not obey the selected noise distribution. As a result, all samples that exceed the truncation thresholds may contain information that can be used in applications, such as neural decoding [11]. Although the method presented here is a proof-of-concept designed for offline analysis, future versions will be adapted for online computation of the truncation thresholds.

The method presented here may be viewed as a cap-fitting algorithm since it discovers a pair of limits within which the cap of the probability density of the samples making up the data fits a probability density model truncated at those limits. The present method has certain advantages over alternative cap-fitting algorithms [14,15]. First, rather than determining the goodness-of-fit of the noise distribution by comparing the empirical

and theoretical distributions at a single percentile, the present method makes the comparison over the entire interval delimited by the truncation thresholds using the KS test. Second, rather than requiring a spike-free data segment for computing the threshold, which may necessitate deleting spikes from the data, the present method processes filtered extracellular data as is. Third, rather than using thresholds that are symmetrical about the mean, the present method does not constrain the truncation thresholds to be symmetrical about any axis. Because of these advantages, the present method is expected to estimate the noise standard deviation more accurately and yield a pair of thresholds that separate signal and noise more successfully than alternative cap-fitting methods.

Truncation thresholds can be computed for any continuous-valued time series, including simulated membrane potential traces. The biophysical processes underlying neuronal spiking can be explored using biophysically realistic computational neuron models [19,20]. Future studies may explore whether truncation thresholds computed for simulated membrane potential traces contain any information about the neuronal spiking threshold or the biophysical processes underlying thereof. If that is found to be the case, then truncation thresholds computed for real intracellular membrane potential recordings may serve as a tool for making inferences about the biophysical processes underlying neuronal spiking.

Developing a method for computing accurate and objective spike detection thresholds is an active research area. The method presented here computes a pair of thresholds that have advantages over the alternatives considered here. Free from constraints of symmetry about the mean or proportionality to an estimated standard deviation, truncation thresholds are defined by the fact that the data they delimit obey a well-defined noise distribution according to the KS test at a specified significance level. Because of their flexibility and statistically precise definition that is entirely data driven, truncation thresholds also allow estimating the noise standard deviation more accurately than alternative methods. These attributes point to the truncation thresholds as an accurate and principled method for spike detection in extracellular recordings.

Acknowledgments

References

[1] Chorev E, Epsztein J, Houweling AR, Lee AK, Brecht M. Electrophysiological recordings from behaving animals–going beyond spikes. Curr Opin Neurobiol 2009; 19: 513-519.

[2] Obien ME, Deligkaris K, Bullmann T, Bakkum DJ, Frey U. Revealing neuronal function through microelectrode array recordings. Front Neurosci 2015; 8: 423.

[3] Buzsáki G. Large-scale recording of neuronal ensembles. Nat Neurosci 2004; 7: 446-451.

[4] Engel AK, Moll CK, Fried I, Ojemann GA. Invasive recordings from the human brain: clinical insights and beyond. Nat Rev Neurosci 2005; 6: 35-47.

[5] Rowland NC, Breshears J, Chang EF. Neurosurgery and the dawning age of Brain-Machine Interfaces. Surg Neurol Int 2013; 4 (Suppl. 1): S11-S14.

[6] Lewicki MS. A review of methods for spike sorting: the detection and classification of neural action potentials. Network 1998; 9: R53-R78.

[7] Quiroga RQ, Nadasdy Z, Ben-Shaul Y. Unsupervised spike detection and sorting with wavelets and superparamagnetic clustering. Neural Comput 2004; 16: 1661-1687.

[8] Vargas-Irwin C, Donoghue JP. Automated spike sorting using density grid contour clustering and subtractive waveform decomposition. J Neurosci Methods 2007; 164: 1-18.

[9] Takekawa T, Isomura Y, Fukai T. Accurate spike sorting for multi-unit recordings. Eur J Neurosci 2010; 31: 263-272.

[10] Jäckel D, Frey U, Fiscella M, Franke F, Hierlemann A. Applicability of independent component analysis on high-density microelectrode array recordings. J Neurophysiol 2012; 108: 334-348.

[11] Todorova S, Sadtler P, Batista A, Chase S, Ventura V. To sort or not to sort: the impact of spike-sorting on neural decoding performance. J Neural Eng 2014; 11: 056005.

[12] Okatan M, Kocatürk, M. Action potential detection in extracellular recordings using "truncation thresholds". In: Medical Technologies National Conference (TIPTEKNO); 15–18 October 2015; Bodrum, Turkey. New York, NY, USA: IEEE. pp. 1-4 (in Turkish with English abstract).

[13] Okatan M, Kocatürk, M. Firing rate dependence of "truncation thresholds". In: Medical Technologies National Conference (TIPTEKNO); 15–18 October 2015; Bodrum, Turkey. New York, NY, USA: IEEE. pp. 1-4 (in Turkish with English abstract).

[14] Thakur PH, Lu H, Hsiao SS, Johnson KO. Automated optimal detection and classification of neural action potentials in extra-cellular recordings. J Neurosci Methods 2007; 162: 364-376.

[15] Yang Z, Liu W, Keshtkaran MR, Zhou Y, Xu J, Pikov V, Guan C, Lian Y. A new EC-PC threshold estimation method for in vivo neural spike detection. J Neural Eng 2012; 9: 046017.

[16] Press WH, Flannery BB, Teukolsky SA, Vetterling WT. Numerical Recipes in C: The Art of Scientific Computing. 2nd ed. Cambridge, UK: Cambridge University Press, 1992.

[17] Kocaturk M, Gulcur HO, Canbeyli R. Toward building hybrid biological/in silico neural networks for motor neuroprosthetic control. Frontiers in Neurorobotics 2015; 9: 8.

[18] Donoho D, Johnstone IM. Ideal spatial adaptation by wavelet shrinkage. Biometrika 1994; 81: 425-455.

[19] Uzun R, Ozer M, Perc M. Can scale-freeness offset delayed signal detection in neuronal networks? Europhys Lett 2014; 105: 60002.

[20] Perc M, Marhl M. Amplification of information transfer in excitable systems that reside in a steady state near a bifurcation point to complex oscillatory behaviour. Phys Rev E 2005; 71: 026229.